Supporting Information for

Multiple strategies of porous tetrametallene for efficient ethanol electrooxidation

Juan Xiong,[a] Hongdong Li,[a] Yue Pan,[a] Jiao Liu,[a] Yan Zhang,[a] Jixiang Xu,[a] Bin Li,[c] Jianping Lai,[,a] and Lei Wang*[,a,b]*

[a] Key Laboratory of Eco-chemical Engineering, Ministry of Education, International Science and Technology Cooperation Base of Eco-chemical Engineering and Green Manufacturing, College of Chemistry and Molecular Engineering, Qingdao University of Science and Technology, Qingdao 266042, P. R. China.

[b] Shandong Engineering Research Center for Marine Environment Corrosion and Safety Protection, College of Environment and Safety Engineering, Qingdao University of Science and Technology, Qingdao 266042, P. R. China.

[c] College of Materials Science and Engineering, Qingdao University of Science and Technology, Qingdao 266061, P. R. China.

*E-mail: jplai@qust.edu.cn (Jianping Lai);inorchemwl@126.com (Lei Wang)

Chemicals: Palladium (II) acetylacetonate ($Pd(acac)_2$, 99%) was purchased from Sigma-Aldrich. Tungsten hexacarbonyl ($W(CO)_6$, 97%) purchased from Alfa Aesar. Rhodium (III) acetylacetonate ($Rh(acac)_3$, 97%) and Bisumuth(III) chloride ($BiCl_3$,98%) were obtained from Sinopharm Chemical Reagent Co. LTD. Potassium hydroxide (KOH, 85%) and acetic acid (CH_3COOH, 99.5%) were obtained from Aladdin. N, N-Dimethylformamide (DMF, 99.5%) and ethanol (CH_3CH_2OH, 99.8%) was obtained from Xilong Scientific Co.,Ltd. All the chemicals were used without further purification. All the solutions were prepared by high purity water (18.2 MΩ cm^{-1}).

Synthesis of porous $Pd_{97}W_3$ porous metallene. For preparation of defect-rich porous $Pd_{97}W_3$ porous nanosheet, 10 mg of $Pd(acac)_2$ and 20 mg of $W(CO)_6$ were added in to a 20 mL of bottle containing 8 mL of DMF, and then sonicated 30 min to get a yellow transparent solution. Afterwards, 2 mL of acetic acid was added into the reaction mixture solution, placing in oil bath at 80 ℃ for 2 h. The obtained black product was collected by centrifugation and washed with ethanol for 3 times, and the defect-rich porous $Pd_{97}W_3$ porous nanosheet was dried at 50 ℃ for further use.

Preparation of PdWM (M = Bi, Rh and RhBi) metallene. The synthesis of PdWM was similar with $Pd_{97}W_3$, except the addition of 6 mg $BiCl_3$ and $Rh(acac)_3$. For $Pd_{66}W_{15}Rh_{12}Bi_7$, $Pd_{61}W_{10}Rh_{17}Bi_{12}$ and $Pd_{59}W_8Rh_{19}Bi_{14}$, the dosage of $BiCl_3$ was changed to 3 mg, 4 mg and 5 mg respectively, the dosage of $Rh(acac)_3$ was changed to 3 mg, 2 mg and 1 mg respectively.

Characterization. The morphologies of the samples were characterized by transmission electron microscopy (TEM) and high-resolution TEM (HRTEM) on an FEI Tecnai-G2 F30 at an accelerating voltage of 300 KV. The high-resolution transmission microscopy (HRTEM) images and energy dispersive X-ray spectroscopy (EDS) were taken by JEOL JEM-F200. Powder X-ray diffraction (XRD) S2 spectra were recorded on an X'Pert-Pro X-ray powder diffractometer equipped with a Cu radiation source (λ = 0.15406 nm). The chemical valence of each element was collected by X-ray photoelectron spectra (XPS) on SSI SProbe XPS Spectrometer. The detection of acetic acid and acetaldehyde were conducted by gas chromatography (GC, SHIMADZU GC2014C). The intermediate products were detected by in-situ FTIR (Thermo iS50 FT-IR).

Electrochemical measurements. Before the electrochemical property tests, the catalyst and carbon black were formed into composites. The obtained 1 mg PdWM were dispersed in 10 mL of cyclohexane and 4 mg carbon (Ketjen Black-300) in 10 mL of ethanol under sonication for 1 h and collected via centrifugation with ethanol. The as-prepared catalysts were dispersed in a mixture of isopropanol, water and 5 wt% Nafion solution (v: v: v = 3: 1: 0.05) with a concentration of 1 mg mL^{-1}. All the electrochemical tests were conducted by CHI 660E electrochemical workstation (Chenhua, Shanghai) with a traditional three-electrode system. The catalysts modified glass carbon electrode was used as working electrode, a Pt foil was used as counter electrode, and a saturated calomel electrode (SCE) was used as reference electrode. The potential was calibrated by the Nernst equation that $E_{(RHE)} = E_{(SCE)} + 0.242 + 0.0592*pH$. Before each test, GCE was polished by Al_2O_3 powder to get a smooth surface. The modified working electrodes were activated by cyclic voltammetry between 0.09-1.3 V (*vs*. RHE) at 500 mV s^{-1} in N_2-saturated 1.0 M KOH for 100 cycles to get a clean catalytic surface. EOR tests were measures in N_2-saturated 1.0 M KOH contained 1.0 M ethanol between 0.09-1.5 V (*vs*. RHE) at 50 mV s^{-1}. For the EOR stability tests, chronoamperometric tests were performed at a fixed potential, and 5,000 CVs were also performed to evaluate the stability of catalysts. The CO stripping tests were carried out by i-t test in CO-saturated 1.0 M KOH at 0.1 V (*vs*. RHE) for 900 s, and then, CO stripping curves were recorded between 0-1.2 V *vs.* RHE at a scan rate of 50 mV s^{-1}.

Calculation of C1 selectivity. The yield of possible EOR product can be conducted by GC and Faradaic formula. Firstly, a series of acetic acid and acetaldehyde standard solutions has been made with a stepped concentration (0.1-5 ppm). The standard curve can be drawn with the integral area of GC peak

and the concentration of standard solution. Secondly, a long time i-t test has been conducted to collect the product to be measure. The concentration of as-produced acetic acid and acetaldehyde can be calculated by the standard curve. Finally, based on the Faradaic formula, the Faradic efficiency of as-produced acetic acid and acetaldehyde can be calculated as follow:

$$FE=(N\times n\times 96485)/Q\times 100\%$$

N is the moles of products, n is the number of electron transfer, Q is the total amount of consumed charge during i-t test. The total FE of EOR was assumed as 100%, the possible C1 selectivity is the residue of C2 pathway.

Electrochemical *in Situ* FTIR reflectance spectroscopy. The intermediate products during the EOR process were detected by *in situ* FTIR through Thermo iS50 FT-IR with a liquid-nitrogen-cooled MCT-A detector. The *in situ* FTIR curves were collected by the method of external reflection. Firstly, the catalysts modified silicon crystal plated with gold was used as working electrode, Ag/AgCl and Pt wire were worked as reference electrode and counter electrode respectively. All the tests were conducted in N_2 saturated 1 M KOH with 1 M ethanol. The applied potential was stepped positively from 0.1 V to 1.2 V (*vs.* RHE) with an interval of 100 mV. Secondly, the results of *in situ* FTIR were reported as relative change in reflectivity: $\Delta R/R = (R(E_S)-R(E_R))/R(E_R)$. The $R(E_S)$ and $R(E_R)$ are the spectra collected at the applied potential and reference potential (0.1 V *vs.* RHE). The upward bands represent the consumption of products, the downward bands represent the formation of reactants.

Figures

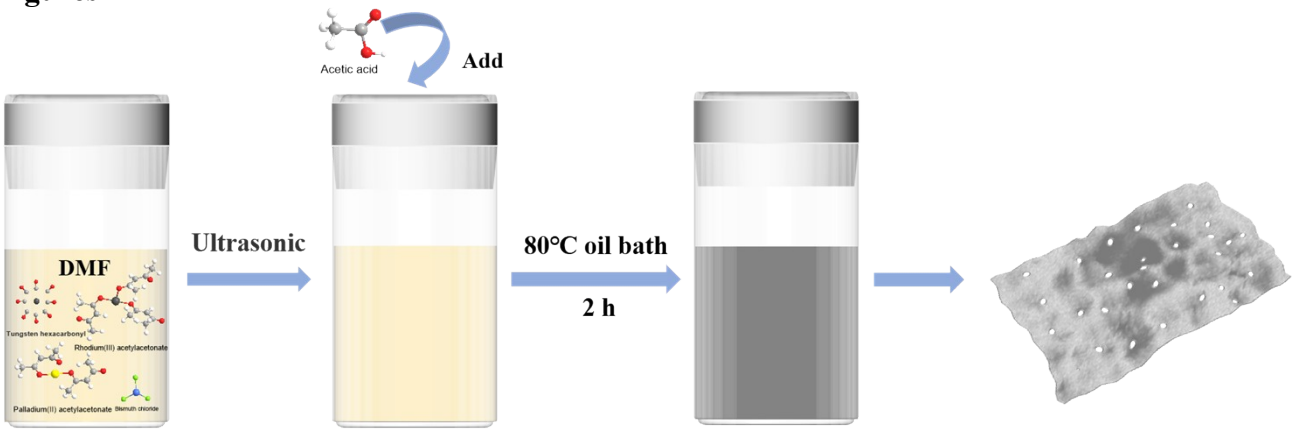

Fig. S1. Schematic illustration for the fabrication of $Pd_{59}W_8Rh_{19}Bi_{14}$ porous metallene.

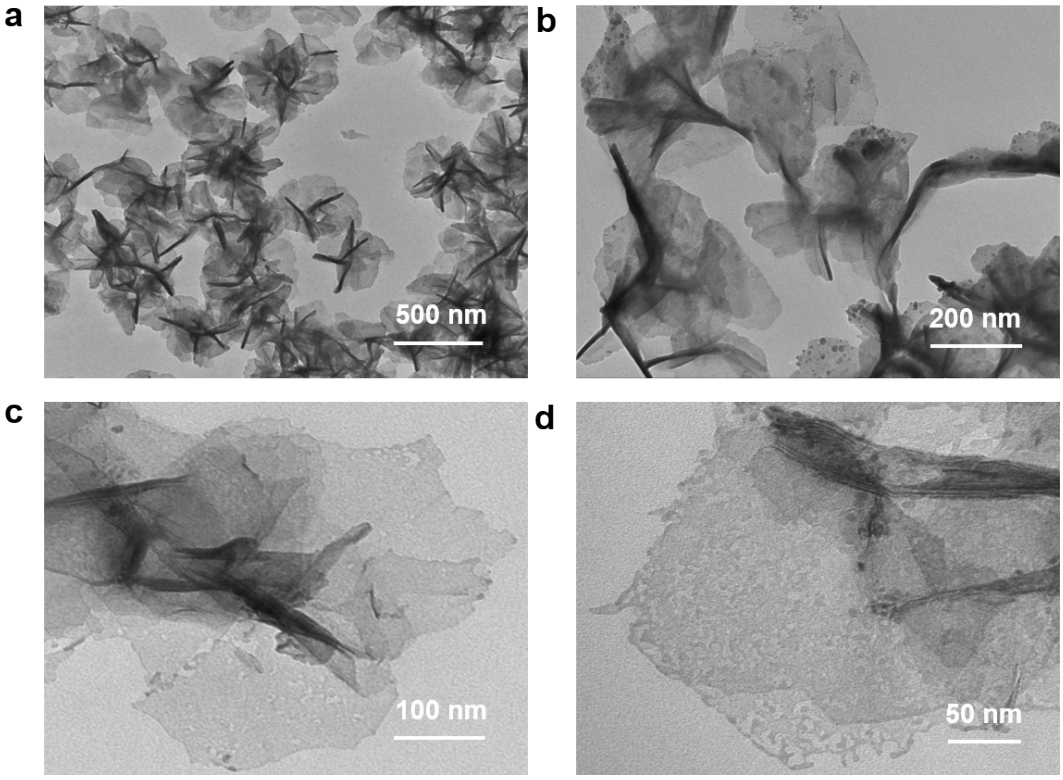

Fig S2. TEM images of $Pd_{59}W_8Rh_{19}Bi_{14}$ metallene at different scales.

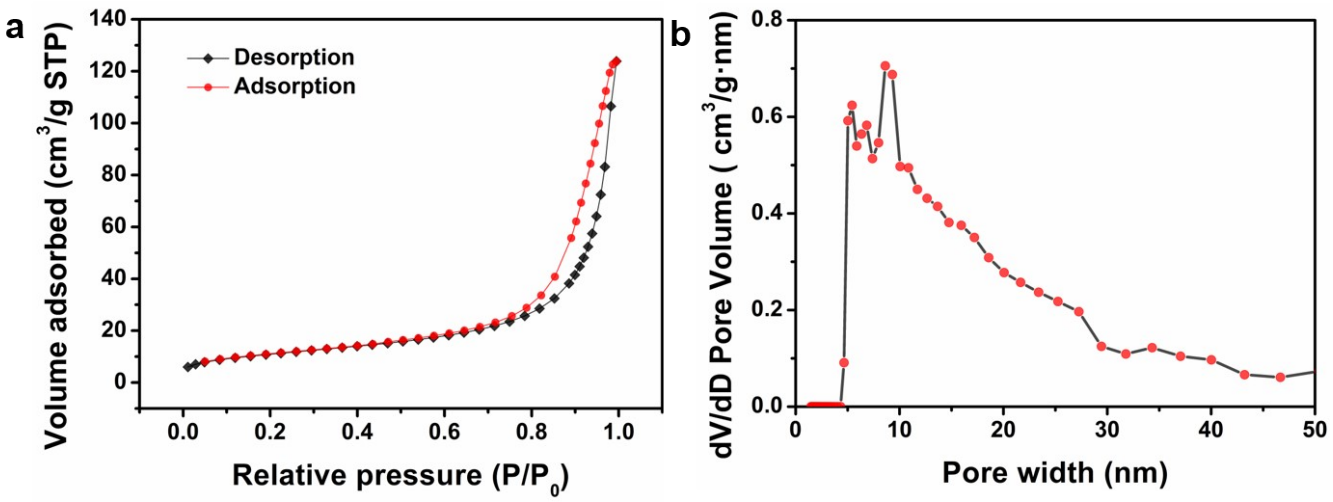

Fig. S3. (a) N_2 adsorption/desorption isotherm curve and (b) derived pore size distribution curves of $Pd_{59}W_8Rh_{19}Bi_{14}$.

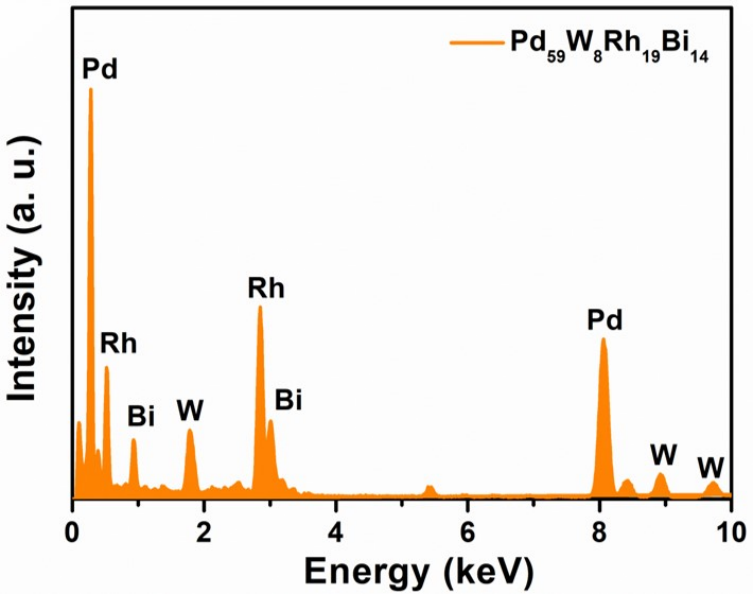

Fig. S4. EDS spectrum of $Pd_{59}W_8Rh_{19}Bi_{14}$.

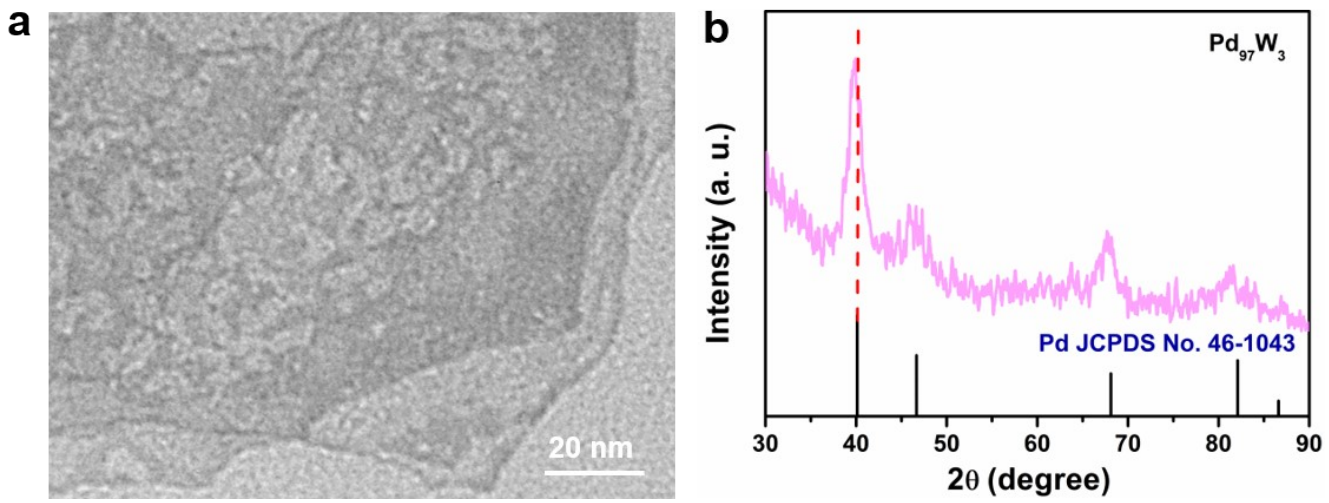

Fig. S5. (a) TEM image and (b) XRD pattern of $Pd_{97}W_3$ porous metallene.

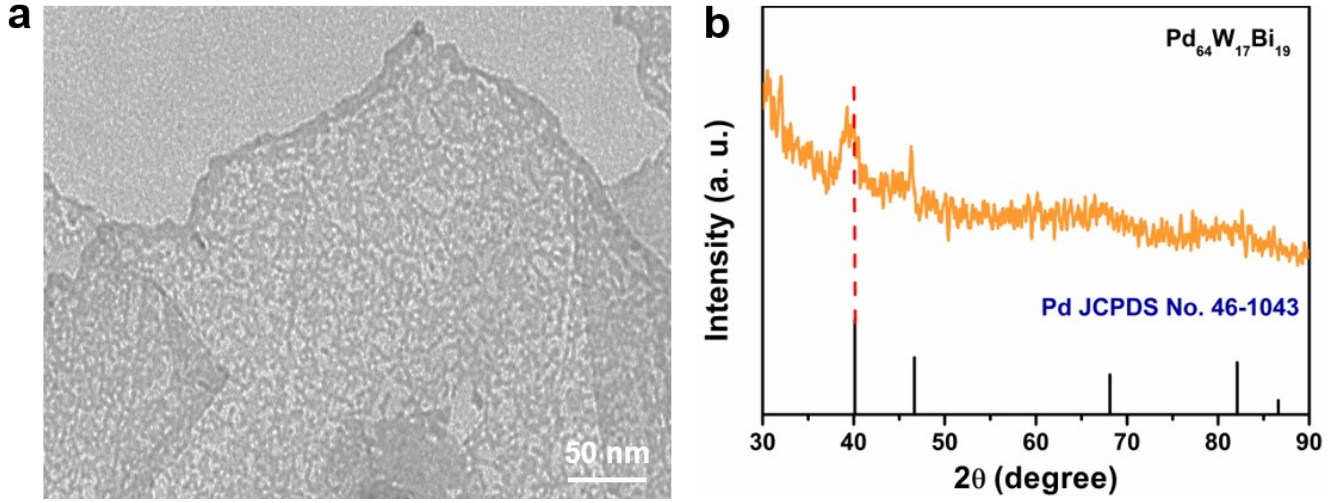

Fig. S6. (a) TEM image and (b) XRD pattern of $Pd_{64}W_{17}Bi_{19}$ porous metallene.

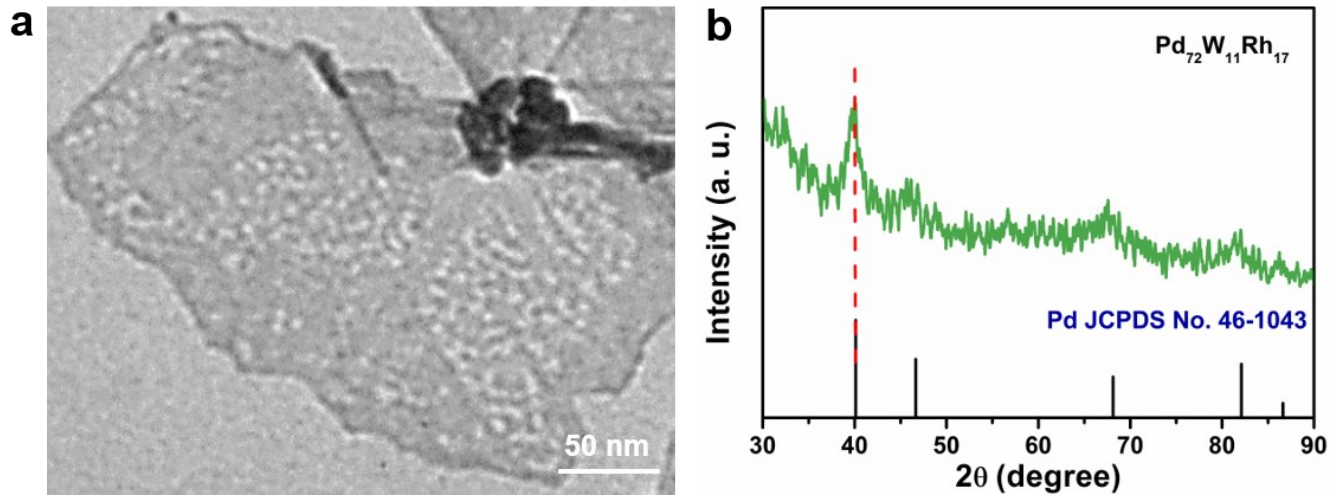

Fig. S7. (a) TEM image and (b) XRD pattern of $Pd_{72}W_{11}Rh_{17}$ porous metallene.

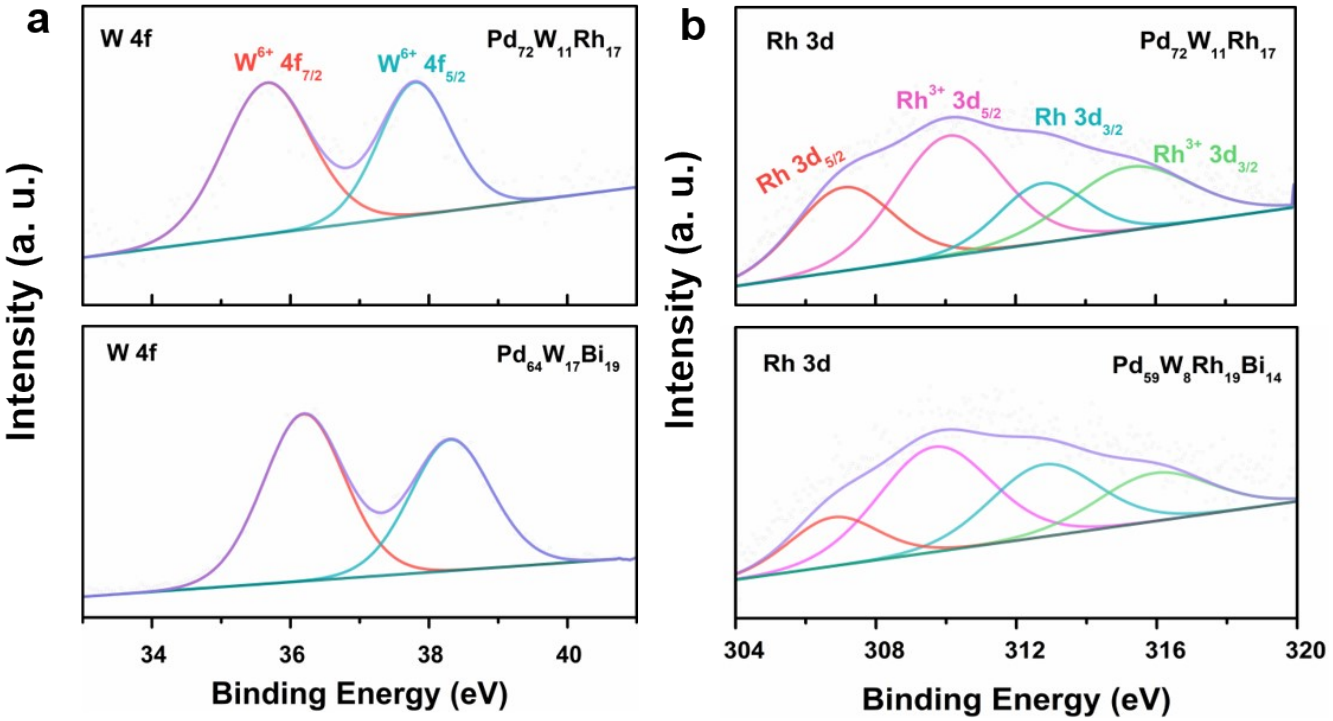

Fig. S8. XPS spectra of as-prepared catalysts. (a) W 4f; (b) Rh 3d.

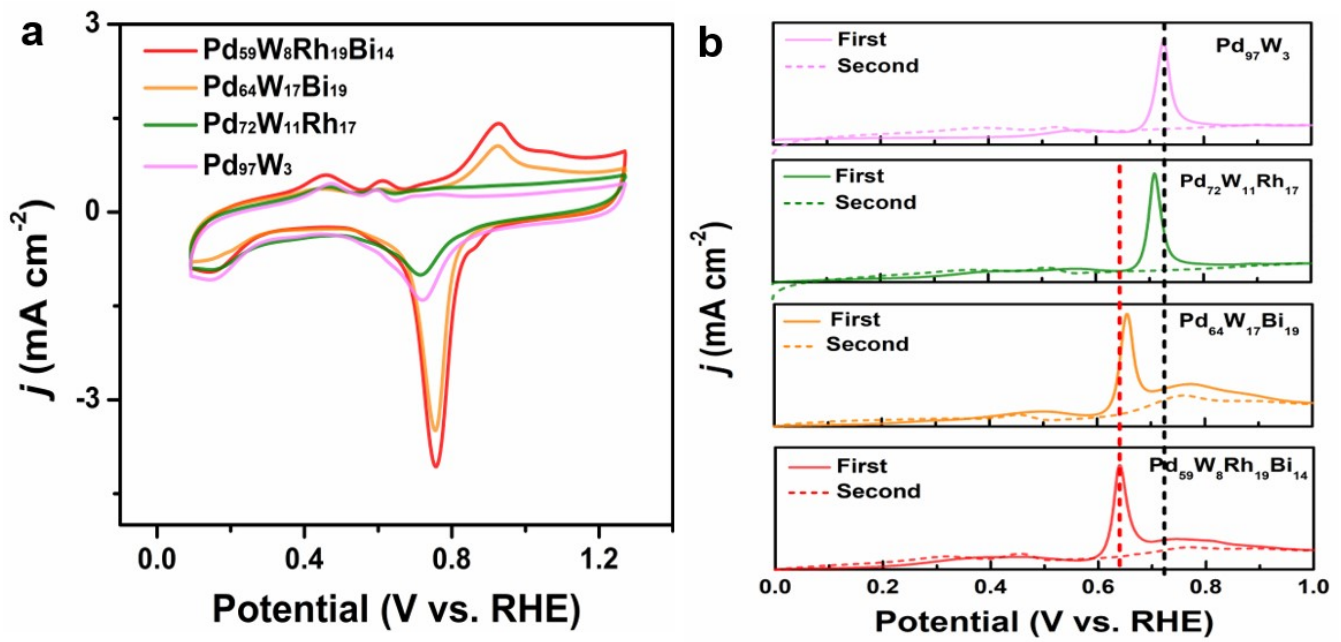

Fig. S9. (a) CV of different electrocatalysts recorded in N_2-saturated 1.0 M KOH. (b) CO stripping curves of different electrocatalysts in 1.0 M KOH electrolyte.

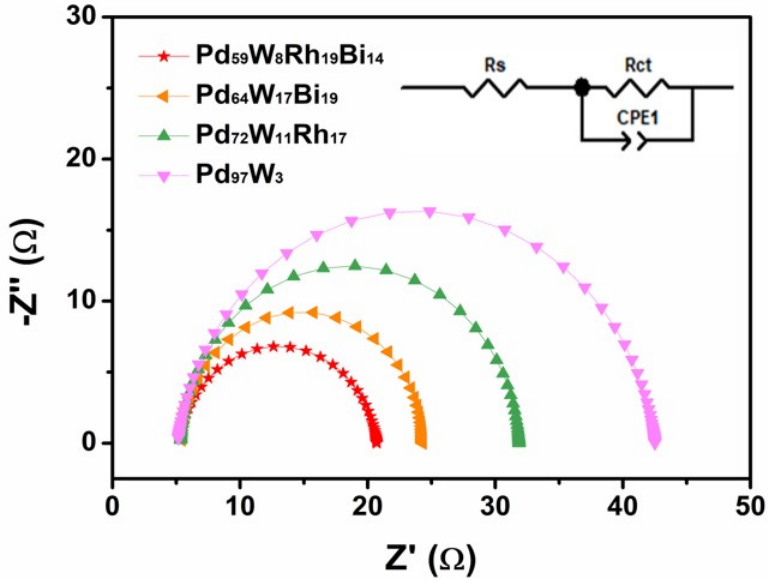

Fig. S10. Nyquist diagram of electrochemical oxidation catalyst in 1.0 M KOH+1.0 M ethanol. Inset: adjust Nyquist diagram to obtain equivalent circuit, where Rs: solution resistance, Rct: charge transfer resistance, CPE: phasing element.

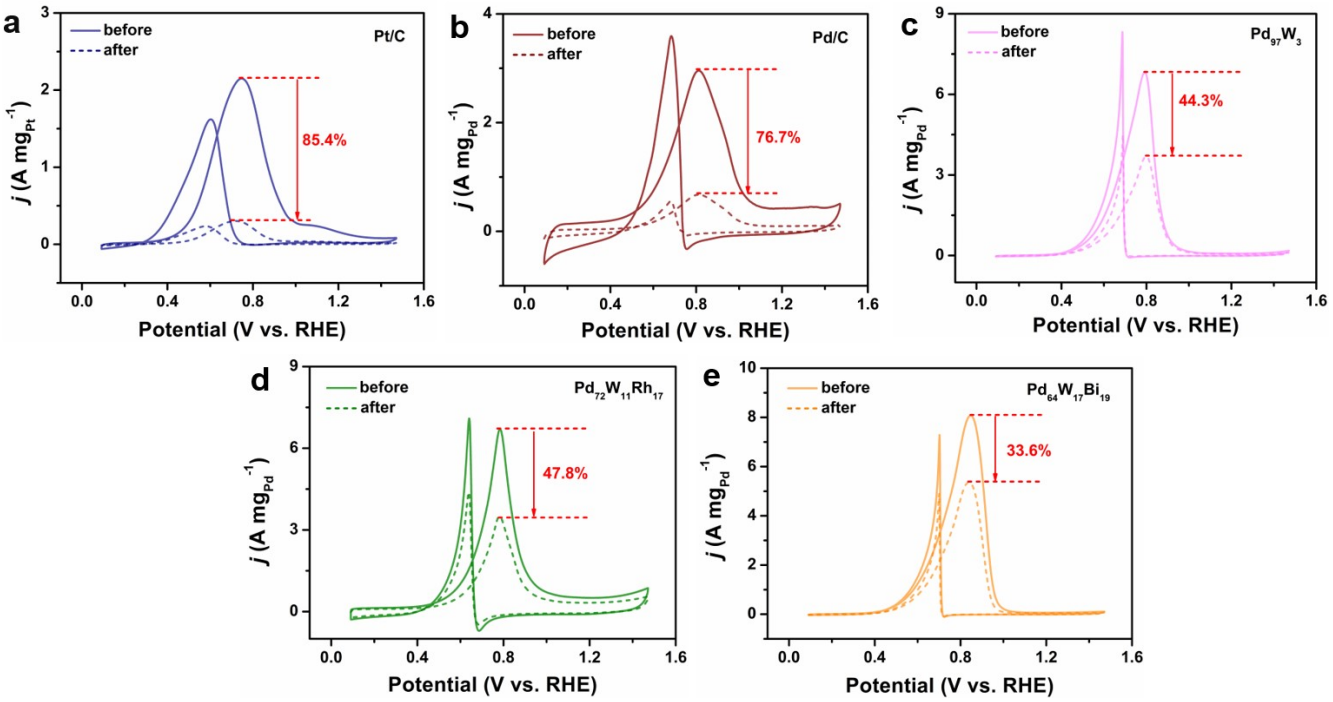

Fig. S11. CV curves of as-prepared catalysts before and after 5000 cycles test. (a) Pt/C; (b) Pd/C; (c) $Pd_{97}W_3$; (d) $Pd_{72}W_{11}Rh_{17}$; (e) $Pd_{64}W_{17}Bi_{19}$.

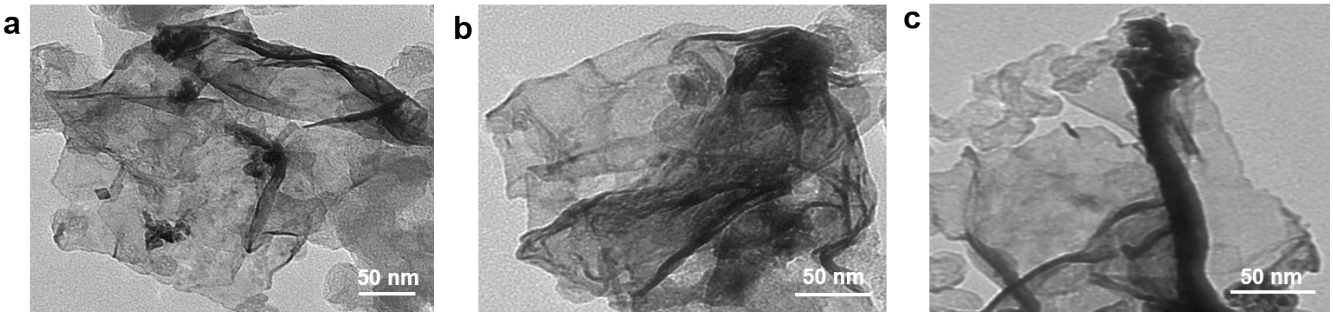

Fig. S12. Representative TEM images of (a) $Pd_{97}W_3$, (b) $Pd_{64}W_{17}Bi_{19}$ and (c) $Pd_{72}W_{11}Rh_{17}$ after EOR stability measurement.

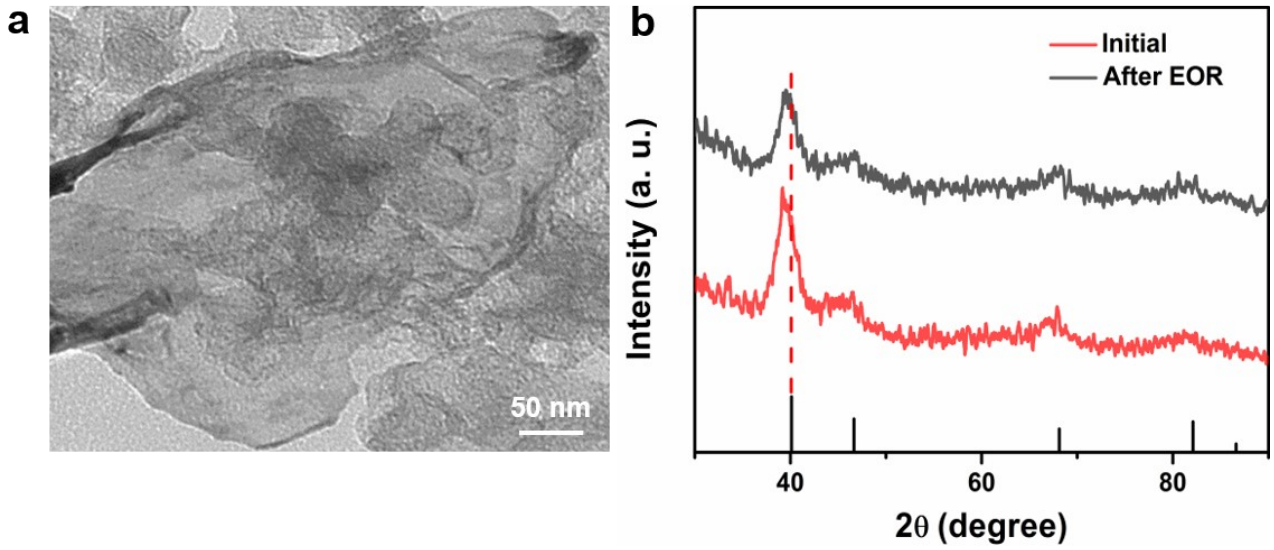

Fig. S13. (a) TEM image of $Pd_{59}W_8Rh_{19}Bi_{14}$ metallene after EOR stability measurement. (b) XRD pattern of the $Pd_{59}W_8Rh_{19}Bi_{14}$ metallene initial and after EOR stability measurement.

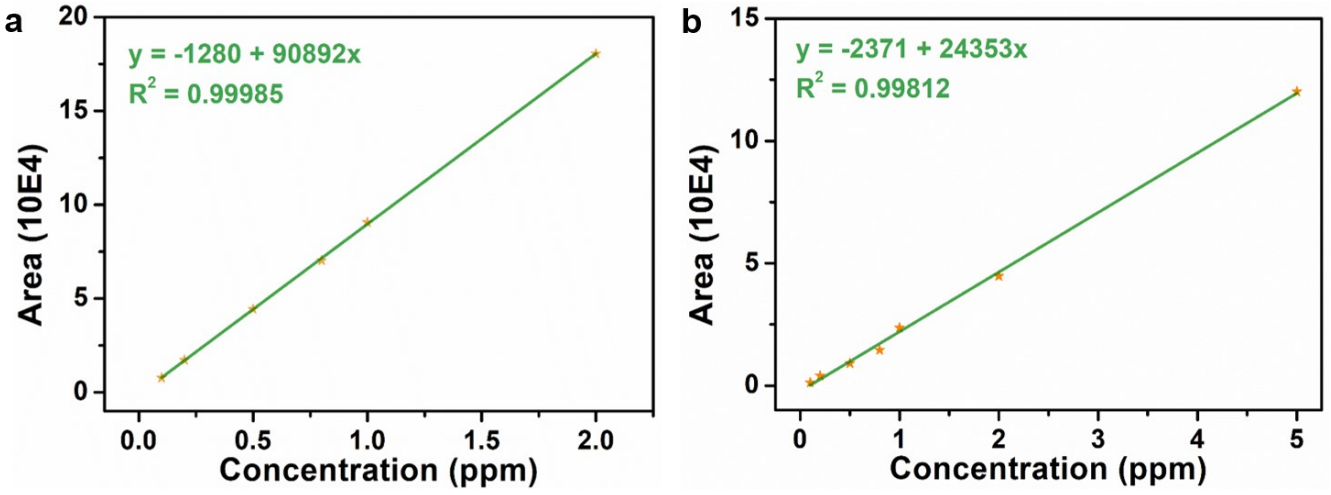

Fig. S14. The standard curves of (a) acetate and (b) acetaldehyde in GC.

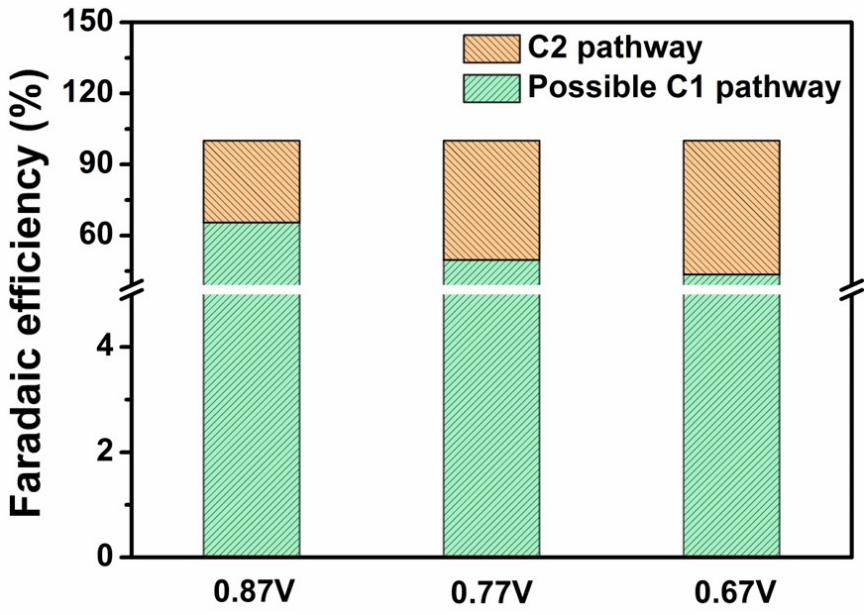

Fig. S15. Faradaic efficiency of $Pd_{59}W_8Rh_{19}Bi_{14}$ at different voltages.

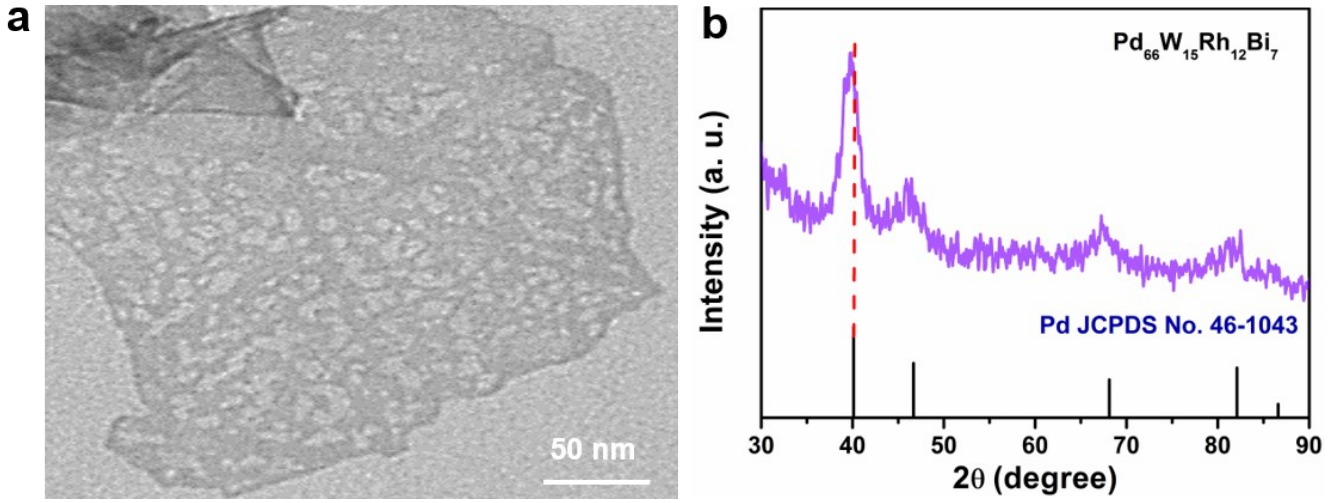

Fig. S16. (a) TEM image and (b) XRD pattern of $Pd_{66}W_{15}Rh_{12}Bi_7$ porous metallene.

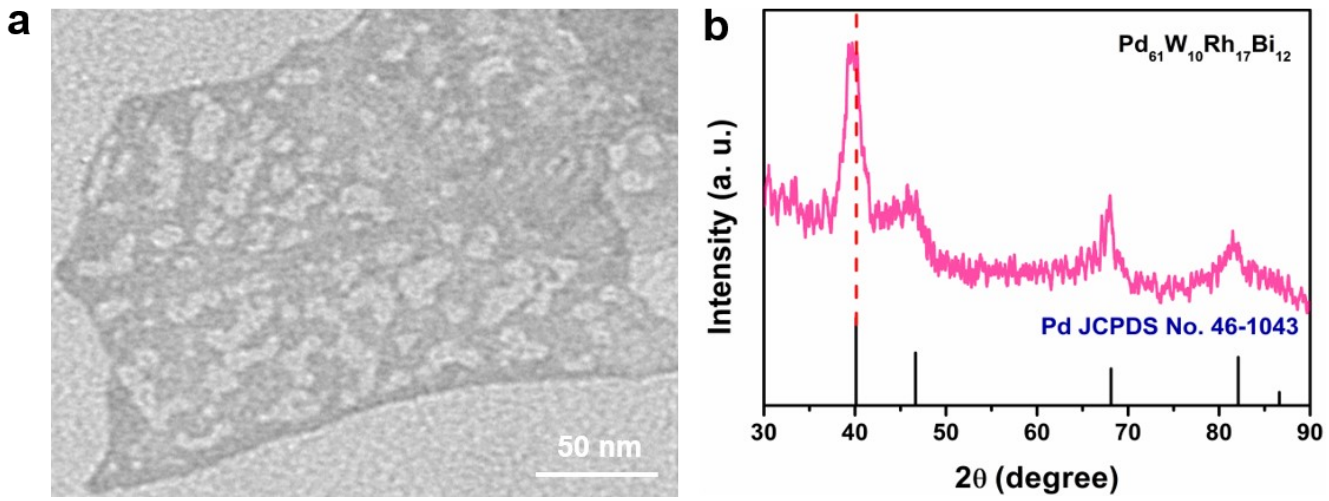

Fig. S17. (a) TEM image and (b) XRD pattern of $Pd_{61}W_{10}Rh_{17}Bi_{12}$ porous metallene.

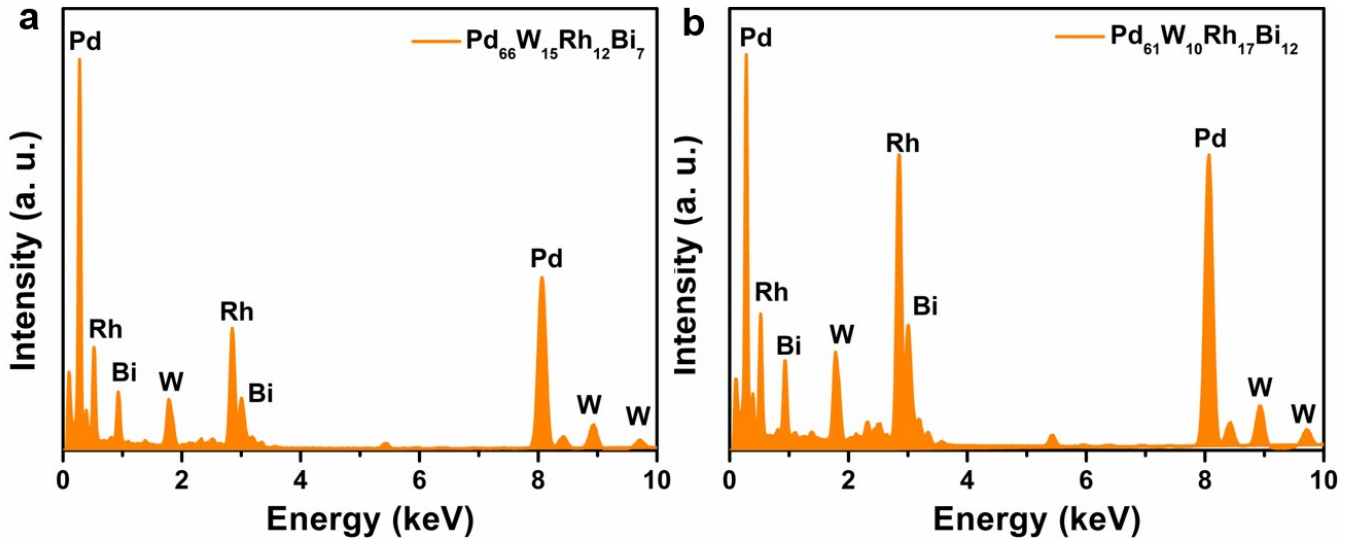

Fig. S18. EDS spectra of (a) $Pd_{66}W_{15}Rh_{12}Bi_7$, (b) $Pd_{61}W_{10}Rh_{17}Bi_{12}$.

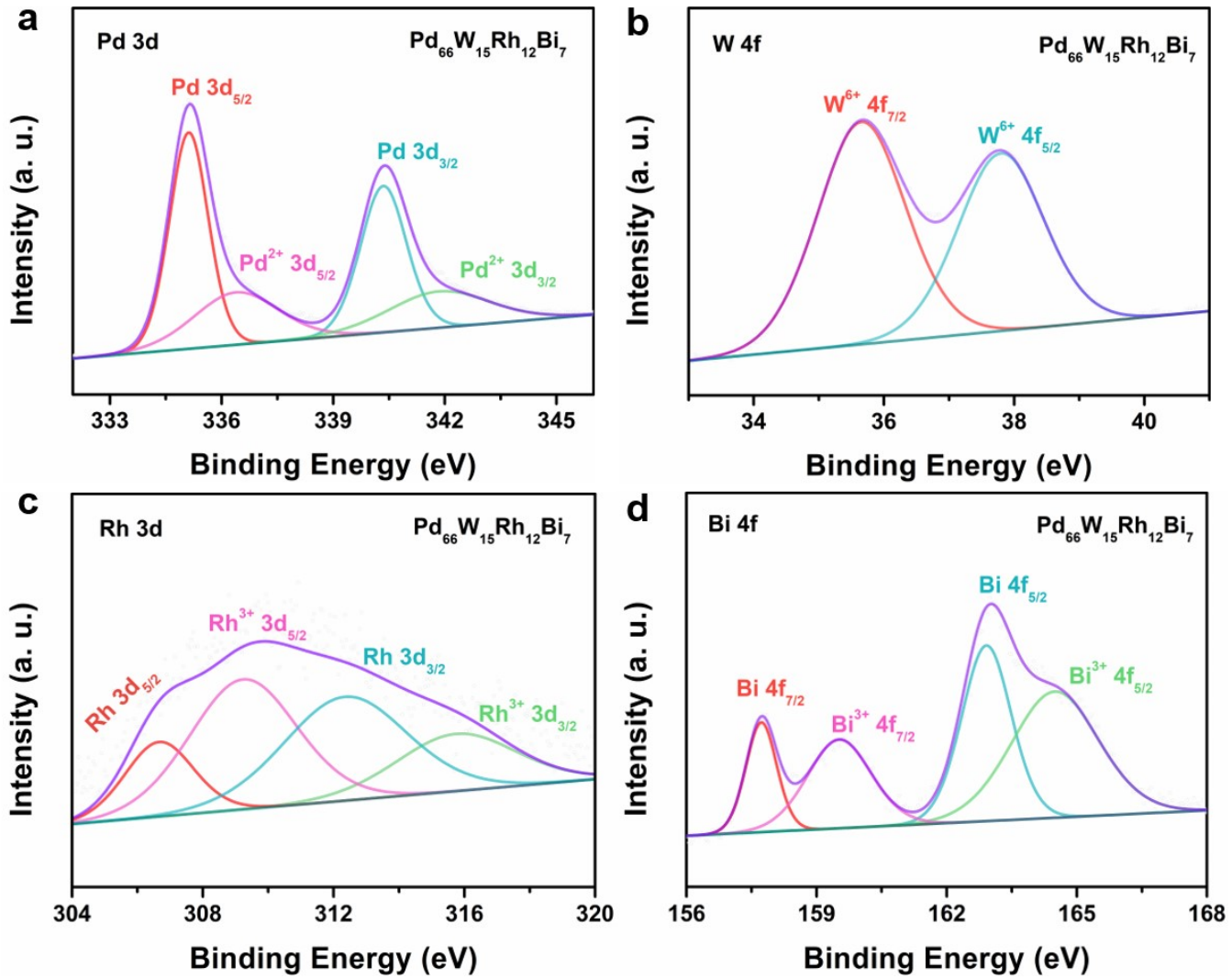

Fig. S19. XPS spectra (a) Pd 3d, (b) W 4f and (c) Rh 3d, (d) Bi 4f of $Pd_{66}W_{15}Rh_{12}Bi_7$.

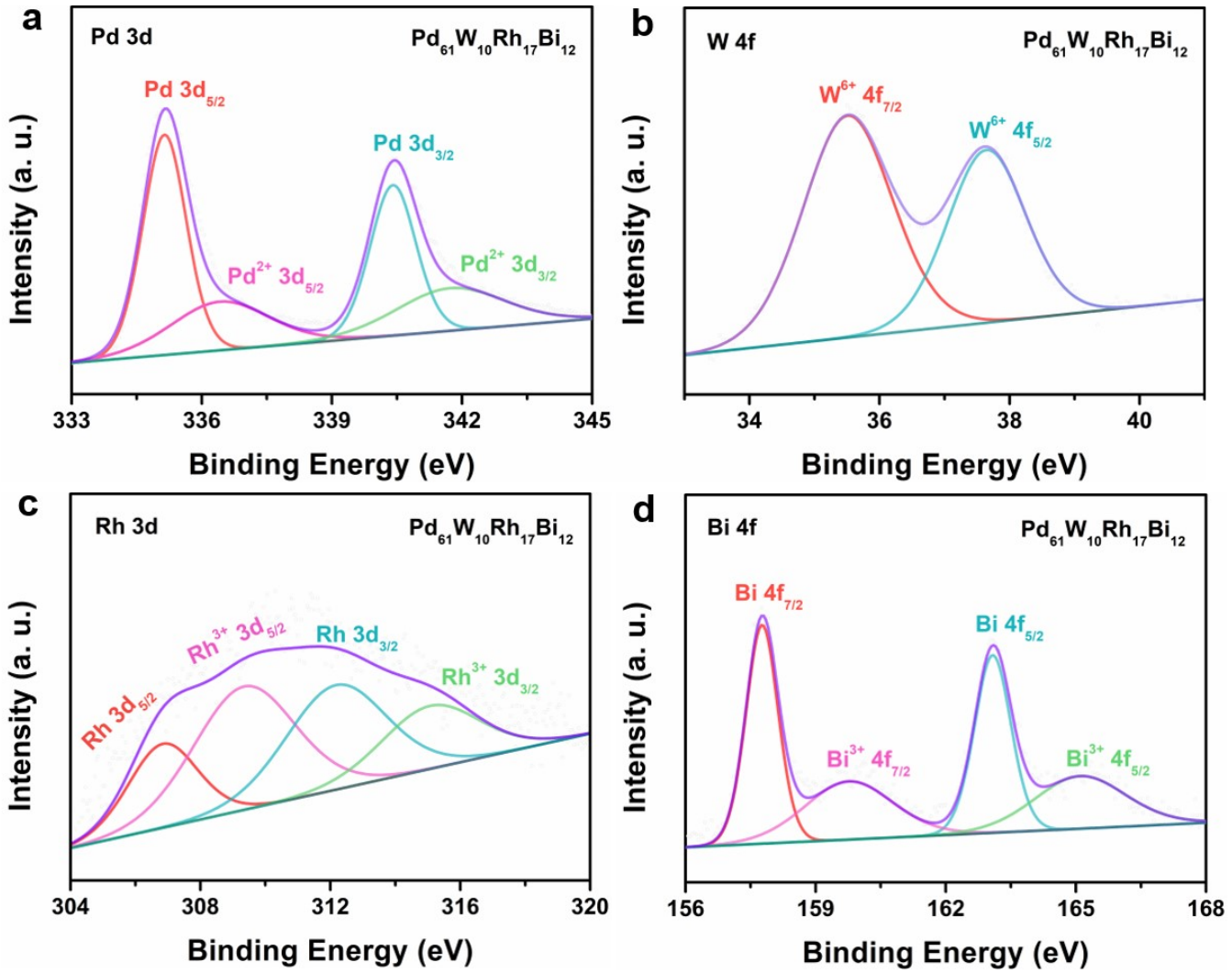

Fig. S20. XPS spectra (a) Pd 3d, (b) W 4f and (c) Rh 3d, (d) Bi 4f of $Pd_{61}W_{10}Rh_{17}Bi_{12}$.

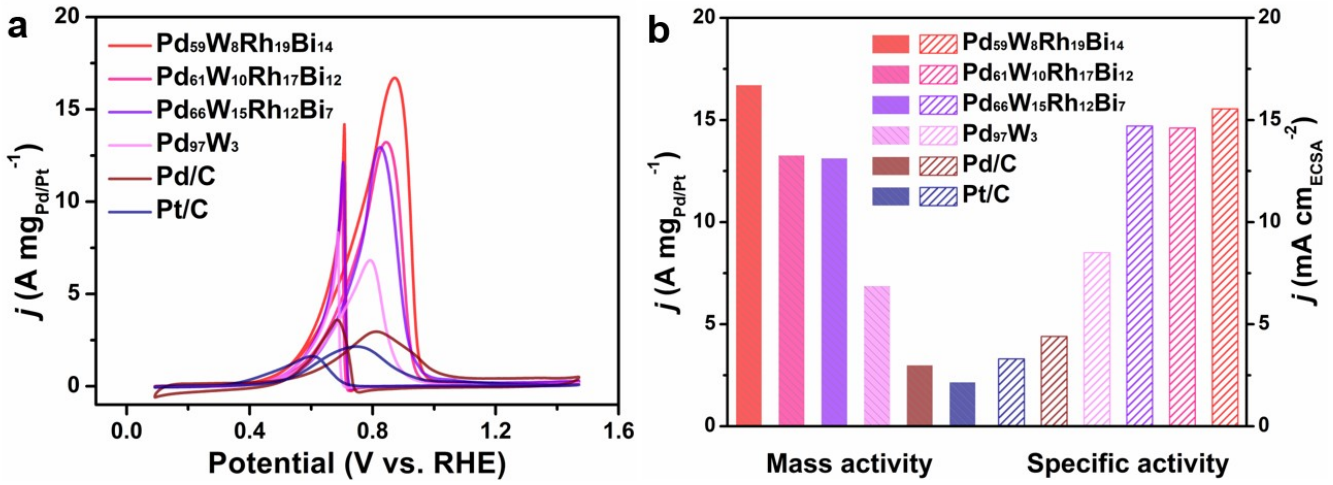

Fig. S21. EOR performance of different electrocatalysts. (a) Mass-normalized EOR CVs. (b) histogram of specific and mass activity for EOR at peak potentials.

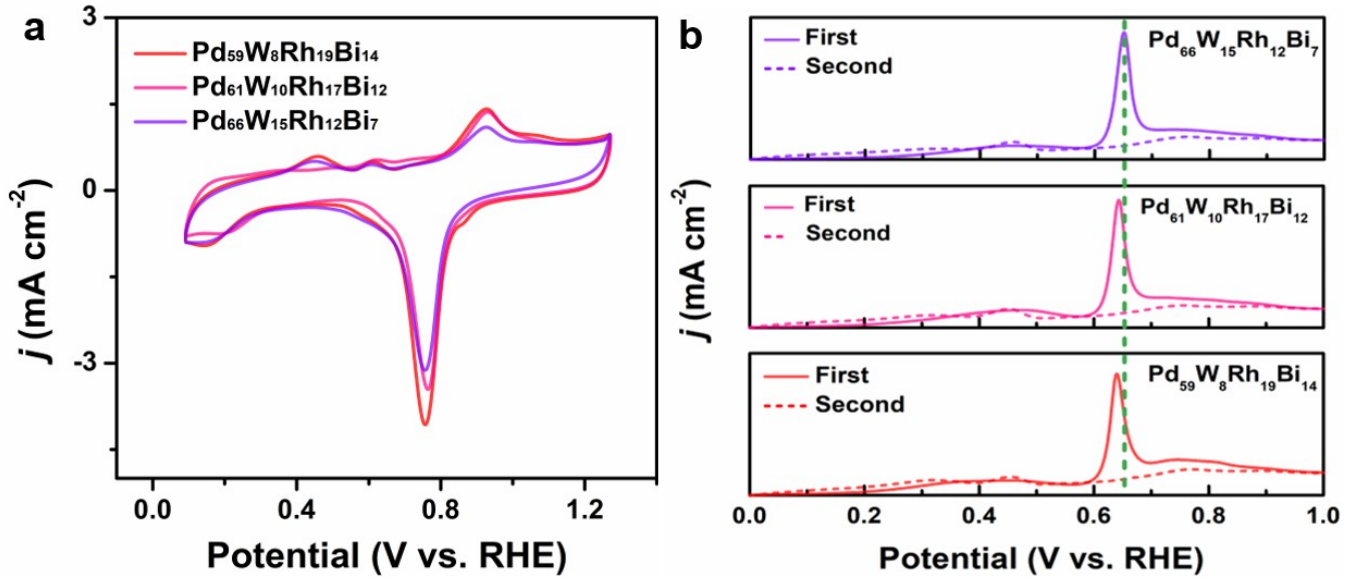

Fig. S22. CO stripping curves of different electrocatalysts in 1.0 M KOH electrolyte.

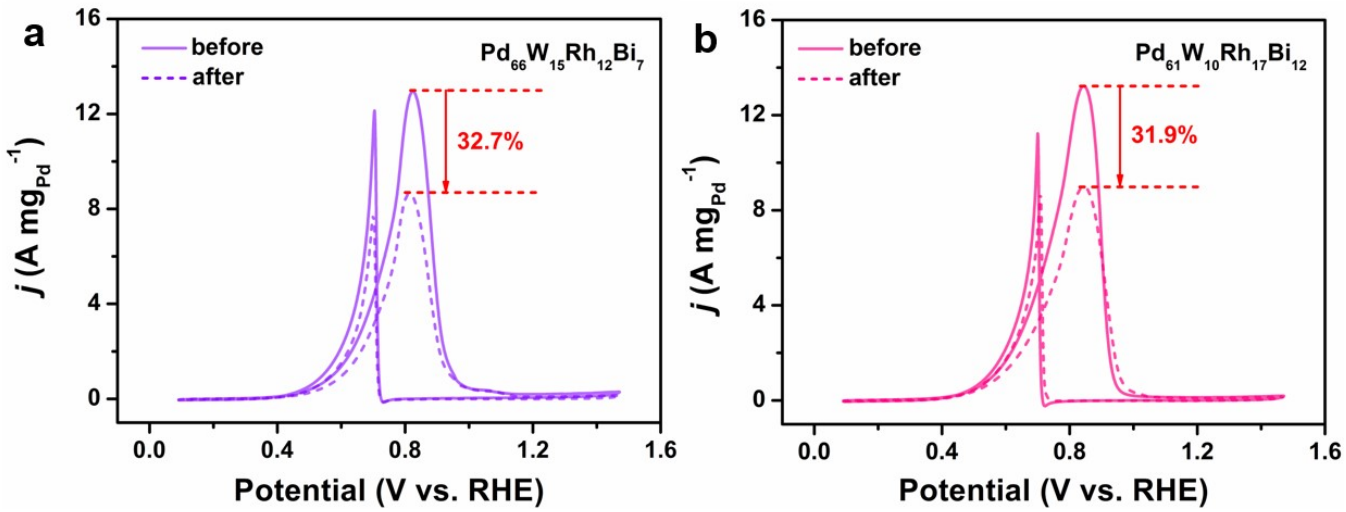

Fig. S23. CV curves of (a) $Pd_{66}W_{15}Rh_{12}Bi_7$ and (b) $Pd_{61}W_{10}Rh_{17}Bi_{12}$ before and after 5000 cycles test.

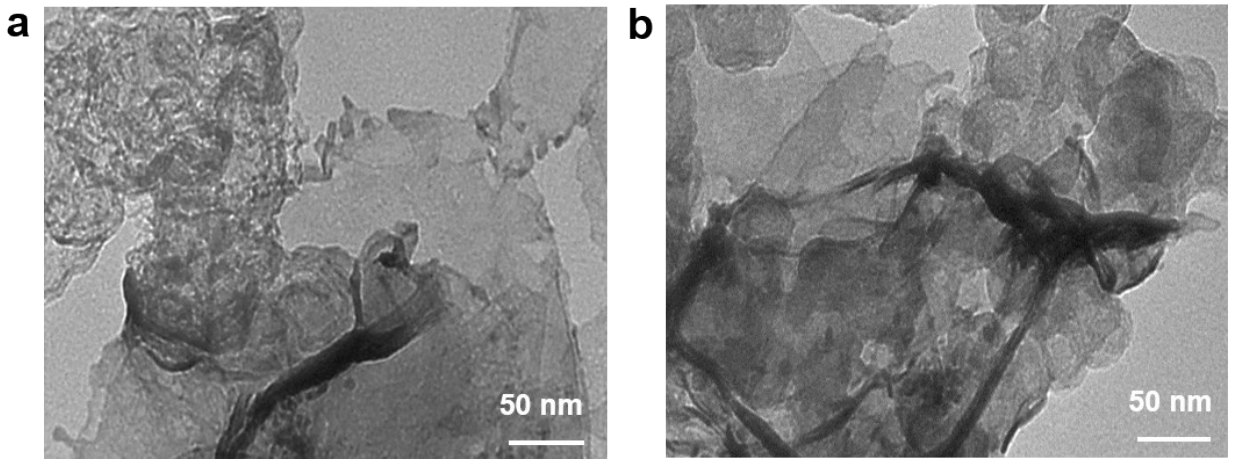

Fig. S24. TEM images of (a) $Pd_{66}W_{15}Rh_{12}Bi_7$ and (b) $Pd_{61}W_{10}Rh_{17}Bi_{12}$ after EOR stability measurement.

Table S1. Atomic ratios of PdWRhBi characterized by ICP.

Samples	Pd atom%	W atom%	Rh atom%	Bi atom%
$Pd_{59}W_8Rh_{19}Bi_{14}$	59.3	7.7	18.6	14.4
$Pd_{61}W_{10}Rh_{17}Bi_{12}$	60.5	10.4	16.8	12.3
$Pd_{66}W_{15}Rh_{12}Bi_7$	66.2	14.6	11.8	7.4

Table S2. ECSA of different electrocatalysts catalysts.

Electrocatalsyts	ECSA / $m^2\ g^{-1}$
Pt/C	73.3
Pd/C	41.5
$Pd_{97}W_3$	80.3
$Pd_{64}W_{17}Bi_{19}$	82.0
$Pd_{72}W_{11}Rh_{17}$	81.5
$Pd_{66}W_{15}Rh_{12}Bi_7$	89.2
$Pd_{61}W_{10}Rh_{17}Bi_{12}$	90.6
$Pd_{59}W_8Rh_{19}Bi_{14}$	107.4

Table S3. A literature survey of the activity and stability of Pd-based EOR electrocatalysts in alkaline electrolytes.

Electrocatalyst	Electrolyte	Mass Activity	Cycling stability	Chronoamperometric stability	Reference
$Pd_{59}W_8Rh_{19}Bi_{14}$	1.0 M KOH + 1.0 M ethanol	16.70 A mg_{Pd}^{-1}	85.3 % activity retention after 5,000 cycles	32% (4.3 A mg^{-1}) activity retention after 20,000 s	This work
Pd-Au HNS	1.0 M KOH + 1.0 M ethanol	8.0A mg_{Pd}^{-1}	89 % activity retention after 2,000 cycles	23% activity retention after 5,000 s	1

$Pd_{50}W_{27}Nb_{23}$/C trimetallene	1.0 M KOH + 1.0 M ethanol	15.6 A mg^{-1}	69.9 % activity retention after 3,000 cycles	15.4 % activity retention after 5,000 s	2
10 nm Pd_3Pb nanocubes	0.5 M KOH + 0.5 M EtOH	4.4 A mg_{Pd}^{-1}	NA	30% activity retention after 1,000 s	3
Pd/Black Phosphorus−graphene	1 M NaOH + 1 M ethanol	6.00 A mg^{-1}	NA	12% (0.71 A mg^{-1}) activity retention after 20,000 s	4
Pd-Ru/TiO_2	1 M NaOH + 1 M ethanol	2.70 A mg^{-1}	NA	29% (0.38 A mg^{-1}) activity retention after 10,000 s	5
PdP_2/rGO	0.5 M KOH + 0.5 M ethanol	1.60 A mg^{-1}	NA	6% (0.05 A mg^{-1}) activity retention after10,000 s	6
PdBi-$Bi(OH)_3$ nanochains	1 M NaOH+ 1 M ethanol	5.30 A mg^{-1}	NA	76 % (2.12 A mg^{-1}) activity retention after 3,600 s, 36 % (1.00 A mg^{-1}) activity retention after 20,000 s	7
PdAg NDs	1.0 M KOH + 1.0 M ethanol	2630 mA mg^{-1}	50% activity retention after 10,000 cycles	52% activity retention after 10,000 s	8
Pd/TiO_2-nanosheets-black P	1 M NaOH + 1 M ethanol	5.02 A mg^{-1}	NA	31% (0.87 A mg^{-1}) activity retention after 3,600 s	9
Pd/$Ni(OH)_2$/rGO	1.0 M KOH + 1.0 M ethanol	1546 mA mg^{-1}	95 % activity retention after 40,000 cycles	76 % activity retention after 3,600s 55 % activity retention after 20,000 s	10
Pd-Ni-P	1 M NaOH + 1 M ethanol	4.95 A mg^{-1}	NA	15% (0.22 A mg^{-1}) activity retention after 2,000 s	11
Au@Pd Nanorods	1 M NaOH + 1 M ethanol	2.92 A mg^{-1}	NA	32% (0.96 A mg^{-1}) activity retention after 1,200 s	12
PdS_x/C	1.0 M KOH + 1.0 M ethanol	162.1 mA mg^{-1}	64.4% activity retention after 3,600 cycles	6 % activity retention after 3,600 s	13
$PdCu_2$	1.0 M KOH + 1.0 M ethanol	1600 m A mg^{-1}	72% activity retention after 300 cycles	43 % activity retention after 1,000 s	14

1

Table S4. I_f/I_b ratio of different electrocatalysts for EOR in alkaline solution.

Electrocatalsyts	I_f/I_b
Pd/C	0.81
$Pd_{97}W_3$	0.82
$Pd_{64}W_{17}Bi_{19}$	1.11
$Pd_{72}W_{11}Rh_{17}$	0.95
$Pd_{66}W_{15}Rh_{12}Bi_7$	1.08
$Pd_{61}W_{10}Rh_{17}Bi_{12}$	1.17
$Pd_{59}W_8Rh_{19}Bi_{14}$	1.18

Table S5. Comparison performance of $Pd_{59}W_8Rh_{19}Bi_{14}$ and other electrocatalysts for EOR activity and Faraday efficiency in alkaline solution.

Catalysts	Electrolyte	Mass Activity	FE of C1 pathway (%)	Reference
$Pd_{59}W_8Rh_{19}Bi_{14}$	1.0 M KOH + 1.0 M ethanol	16.70A mg_{Pd}^{-1}	65.41	This work
Pd-Au HNS	1.0 M KOH + 1.0 M ethanol	8.0 A mg^{-1}_{Pd}	33.2	1
$Pd_{50}W_{27}Nb_{23}$/C trimetallene	1.0 M KOH + 1.0 M ethanol	15.6 A mg^{-1}_{Pd}	55.5	2
RhPb-PbO_2/C	1.0 M NaOH+ 1.0 M ethanol	2.64 A mg^{-1}	20	15
CoP/RGO-Pd	1.0 M KOH + 1.0 M ethanol	4.60 A mg^{-1}	27.6	16
Ag@$Pd_2P_{0.2}$	1.0 M KOH + 1.0 M ethanol	7.24A mg^{-1}	19	17
$Pt_{54}Rh_4Cu_{42}$ CNBs	1.0 M KOH + 1.0 M ethanol	4.09 A mg^{-1}	40.7	18
Pd/$Ni(OH)_2$/rGO	1.0 M KOH + 1.0 M ethanol	1.5 A mg^{-1}	26	10

References

1. F. Lv, W. Zhang, M. Sun, F. Lin, T. Wu, P. Zhou, W. Yang, P. Gao, B. Huang and S. Guo, *Adv. Energy Mater.*, 2021, **11**, 2100187.
2. Y. Qin, H. Huang, W. Yu, H. Zhang, Z. Li, Z. Wang, J. Lai, L. Wang and S. Feng, *Adv. Sci.*, 2022, **9**, 2103722.
3. X. Yu, Z. Luo, T. Zhang, P. Tang, J. Li, X. Wang, J. Llorca, J. Arbiol, J. Liu and A. Cabot, *Chem. Mater.*, 2020, **32**, 2044-2052.
4. T. Wu, Y. Ma, Z. Qu, J. Fan, Q. Li, P. Shi, Q. Xu and Y. Min, *ACS Appl. Mater. Interfaces*, 2019, **11**, 5136-5145.
5. X. Liu, L. Ning, M. Deng, J. Wu, A. Zhu, Q. Zhang and Q. Liu, *Nanoscale*, 2019, **11**, 3311-3317.
6. J. Liu, Z. Luo, J. Li, X. Yu, J. Llorca, D. Nasiou, J. Arbiol, M. Meyns and A. Cabot, *Appl. Catal. B: Environ.*, 2019, **242**, 258-266.
7. X. Yuan, Y. Zhang, M. Cao, T. Zhou, X. Jiang, J. Chen, F. Lyu, Y. Xu, J. Luo, Q. Zhang and Y. Yin, *Nano Lett.*, 2019, **19**, 4752-4759.
8. W. Huang, X. Kang, C. Xu, J. Zhou, J. Deng, Y. Li and S. Cheng, *Adv. Mater.*, 2018, **30**, 1706962.
9. T. Wu, J. Fan, Q. Li, P. Shi, Q. Xu and Y. Min, *Adv. Energy Mater.*, 2017, **8**, 1701799.
10. W. Huang, X. Ma, H. Wang, R. Feng, J. Zhou, P. Duchesne, P. Zhang, F. Chen, N. Han, F. Zhao, J. Zhou, W. Cai and Y. Li, *Adv. Mater.*, 2017, **29**, 1703057.
11. L. Chen, L. Lu, H. Zhu, Y. Chen, Y. Huang, Y. Li and L. Wang, *Nat. Commun.*, 2017, **8**, 14136.
12. Y. Chen, Z. Fan, Z. Luo, X. Liu, Z. Lai, B. Li, Y. Zong, L. Gu and H. Zhang, *Adv. Mater.*, 2017, **29**, 1701331.
13. Q. Zhang, F. Zhang, X. Ma, Y. Zheng and S. Hou, *J. Power Sources*, 2016, **336**, 1-7.
14. J. Xue, G. Han, W. Ye, Y. Sang, H. Li, P. Guo and S. Zhao, *ACS Appl. Mater. Interfaces*, 2016, **8**, 34497-34505.
15. B. Lan, M. Huang, L. Wei, N. Wang, L. Wang and Y. Yang, *Small*, 2020, **16**, e2004380.
16. M. Wang, R. Ding, Y. Xiao, H. Wang, L. Wang, C. Chen, Y. Mu, G. Wu and B. Lv, *ACS Appl. Mater. Interfaces*, 2020, **12**, 28903-28914.
17. X. Yang, Z. Liang, S. Chen, M. Ma, Q. Wang, X. Tong, Q. Zhang, J. Ye, L. Gu and N. Yang, *Small*, 2020, **16**, e2004727.
18. S. Han, H. Liu, P. Chen, J. Jiang and Y. Chen, *Adv. Energy Mater.*, 2018, **8**, 1801326.